# A Systematic Examination of the Morphogenesis of Calcium Carbonate in the Presence of a Double-Hydrophilic Block Copolymer

**Helmut Cölfen* and Limin Qi[a]**

**Abstract:** In this paper, a systematic study of the influence of various experimental parameters on the morphology and size of $CaCO_3$ crystals after room-temperature crystallization from water in the presence of poly(ethylene glycol)-*block*-poly(methacrylic acid) (PEG-*b*-PMAA) is presented. The pH of the solution, the block copolymer concentration, and the ratio [polymer]/[$CaCO_3$] turned out to be important parameters for the morphogenesis of $CaCO_3$, whereas a moderate increase of the ionic strength (0.016 M) had no influence. Depending on the experimental conditions, the crystal morphologies can be tuned from calcite rhombohedra via rods, ellipsoids or dumbbells to spheres. A morphology map is presented which allows the prediction of the crystal morphology from a combination of pH, and $CaCO_3$ and polymer concentration. Morphologies reported in literature for the same system but under different crystallization conditions agree well with the predictions from the morphology map. A closer examination of the growth of polycrystalline macroscopic $CaCO_3$ spheres by TEM and time-resolved dynamic light scattering showed that $CaCO_3$ macrocrystals are formed from strings of aggregated amorphous nanoparticles and then recrystallize as dumbbell-shaped or spherical calcite macrocrystal.

**Keywords:** aggregation · block copolymers · calcium · calcium carbonate · colloids · morphogenesis

## Introduction

The synthesis of inorganic materials of specific size and morphology is a key aspect in fields as diverse as modern materials, catalysis, medicine, electronics, ceramics, pigments, and cosmetics.[1–4] Compared with the size control, the morphology control or morphogenesis is more demanding to achieve by means of classical procedures of colloid chemistry.[5] Biological systems, on the other hand, use organic molecules (mostly proteins and polysaccharides) that function variously as nucleators, cooperative modifiers, and as matrices or molds for minerals. They exert exact control over the processes of biomineralization, which results in unique inorganic–organic hybrids (e.g., seashells, bone, teeth, diatomea, and many others) with their structure, size, and morphology regulated to optimally fit their functions as materials.[6–10] The strategy that organic additives and/or templates with complex functionalization patterns are used to control the nucleation, growth, and alignment of inorganic crystals has been universally applied for the biomimetic synthesis of inorganic materials with complex form.[1]

[a] Dr. H. Cölfen, Dr. L. Qi
Max Planck Institute of Colloids and Interfaces
Colloid Chemistry, Research Campus Golm
14424 Potsdam (Germany)
Fax: (+49) 331-567-9502
E-mail: coelfen@mpikg-golm.mpg.de

One of the most intensely examined systems is calcium carbonate ($CaCO_3$), which is abundant in biominerals, but also of industrial importance due to its wide use as a filler in paints, plastics, rubber, or paper.[11] Among more than 60 known biominerals, the two polymorphs of $CaCO_3$, calcite and aragonite, are by far the most common, whereas vaterite, a less stable polymorph, is not commonly formed by organisms.[12, 13] Biomimetic synthesis of $CaCO_3$ crystals in the presence of organic templates and/or additives has been intensively investigated in recent years. Langmuir monolayers,[14–18] ultrathin organic films,[19] self-assembled films,[20–22] and foam lamellae[23] have been used as effective templates for the controlled growth of $CaCO_3$ crystals, focussing on the control of the polymorph and crystal orientation. Crosslinked gelatin films,[24, 25] polymer substrates,[11] and crystal-imprinted polymer surfaces[26] have also recently been used to direct the controlled growth of $CaCO_3$ crystals. It has been shown that special functional low molecular weight and polymeric additives exhibit large influences on the crystallization of $CaCO_3$.[27–30] $CaCO_3$ films have been successfully prepared in the presence of both organic substrates and soluble polymeric additives.[31, 32] The protein macromolecules isolated from mollusk shells[12, 33, 34] and intracrystalline macromolecules from sea urchin spines[35] have shown distinct control on the polymorph of $CaCO_3$ crystals. Interestingly, a designed peptide has been synthesized and used for the conformation-dependent control of the calcite morphology.[13] More-



0947-6539/01/0701-0106 $ 17.50+.50/0

over, emulsion foams,[36] water-in-oil microemulsions,[37] pseudovesicular double emulsions,[38] and gold colloids[39] have been used as templates to achieve the morphogenesis of $CaCO_3$ with complex morphologies.

Recently, a new class of functional polymers, the so-called double-hydrophilic block copolymers[40] was developed for mineralization purposes. These polymers consist of one hydrophilic block designed to interact strongly with the appropriate inorganic minerals and surfaces, and another hydrophilic block that does not interact (or only weakly) with mineral surfaces and mainly promotes solubilization in water. Owing to the separation of the binding and the solvating moieties, these polymers turned out to be extraordinarily effective in crystallization control for calcium carbonate,[40–42] calcium phosphate,[43] barium sulfate,[44, 45] and zinc oxide.[46] For example, calcite or vaterite spheres, twins, and hollow spheres were obtained.[41] These preliminary experiments, however, seem to be part of a more complex overall scenario, since other authors have used similar polymers, but observed under other operating conditions elongated calcite particles.[42]

It is therefore the aim of the present paper to vary a range of accessible parameters, namely pH, polymer concentration, ionic strength, and the relative amount of mineral to polymer for one distinct polymer, a double-hydrophilic block copolymer of the type PEG-*b*-PMAA, to shed light on the ways how the polymer influences the calcium carbonate growth. It will be shown that a whole "zoo" of rather archetypic morphologies of calcite, such as rods, ellpsoids, spheres, twinned superstructures, and dumbbells can be obtained at room temperature by a simple solution synthesis.

## Experimental Section

**Materials**: Unless otherwise stated, all chemicals were obtained from Aldrich and used without further purification. Homopolymers poly(ethylene glycol) monomethyl ether (PEG, MW = 5000 g mol$^{-1}$) and poly(methacrylic acid, sodium salt) (PMAA, MW = 6500 g mol$^{-1}$) were purchased from Polysciences and Aldrich, respectively. A commercial block copolymer poly(ethylene glycol)-*block*-poly(methacrylic acid) (PEG-*b*-PMAA, PEG = 3000 g mol$^{-1}$, PMAA = 700 g mol$^{-1}$) was obtained from Goldschmidt, Essen (Germany). The copolymer was purified by exhaustive dialysis before it was used in the crystallization of calcium carbonate.

**Crystallization of $CaCO_3$**: The precipitation of $CaCO_3$ was carried out in glass vessels at room temperature (ca. 22 °C). Aqueous solutions of $Na_2CO_3$ (0.5 M) and of $CaCl_2$ (0.5 M) were first prepared as stock solutions. In a typical synthesis, a solution of $Na_2CO_3$ (0.5 M, 0.32 mL) was injected into an aqueous solution of PEG-*b*-PMAA (20 mL, 0.2 g L$^{-1}$) and the pH of the solution was adjusted to a desired pH (e.g., pH 10) by using HCl or NaOH. Then a solutuion of $CaCl_2$ (0.5 M, 0.32 mL) was injected quickly into the pH-adjusted solution under vigorous stirring by using a magnetic stirrer; this gave a final $CaCO_3$ concentration of 8 mM. The mixture was stirred for 1 min, and then the solution was covered and allowed to stand under static conditions for a time of 24 h (unless otherwise specified) before the product was collected for characterization. In the experiments, the starting pH was varied from 11 to 9, the concentration of PEG-*b*-PMAA was varied from 1 to 0.05 g L$^{-1}$ (50 – 1000 ppm), and the final concentration of $CaCO_3$ was varied from 16 to 4 mM. As reference experiments, the homopolymers PEG and PMAA were used in the crystallization experiments to replace the copolymer PEG-*b*-PMAA, with all the other conditions kept the same.

**Characterization**: The resulting $CaCO_3$ precipitates were characterized by scanning electron microscopy (SEM) on a DSM 940 A (Carl Zeiss, Jena) microscope and by transmission electron microscopy (TEM) with a Zeiss EM 912 Omega microscope. Thin-section samples (~50 nm in width) for TEM were prepared by polymerization in epoxy resin followed by cutting with a Leica Ultracut UCT ultramicrotome. Powder X-ray diffraction (XRD) patterns were recorded on a PDS 120 diffractometer (Nonius GmbH, Solingen) with $Cu_{K\alpha}$ radiation. Infrared spectra were collected by using a Nicolet Impact 400 FTIR spectrometer on KBr pellets. The dynamic light scattering (DLS) experiments were performed with a laboratory-built goniometer with temperature control (±0.05 K), an attached single-photon detector ALV/SO-SIPD, and a multiple tau digital correlator ALV 5000/FAST from ALV (Langen, Germany). The light source was an INNOVA 300 argon-ion laser operated at $\lambda = 488.0$ nm in single-frequency mode and powered at approximately 800 mW. The light-scattering quartz cuvette cells (Hellma, Mülheim/Germany) were charged with the freshly prepared stock solutions by directly filtering them through ANOTOP filters (Merck, Germany) with 800 nm pore size. By recording the correlation functions every 30 seconds for approximately 180 min, the onset of timing of our experiments was synchronized with the event of mixing the solution.

## Results

Figure 1 shows the typical electron microscopy (EM) pictures of $CaCO_3$ particles obtained in the presence of the homopolymers PEG and PMAA, and the copolymer PEG-*b*-PMAA under the standard synthesis condition with a polymer concentration of 0.2 g L$^{-1}$, a $CaCO_3$ concentration of 8 mM, and a starting pH of 10.

Similar to the case of the control experiment in which no polymeric additives were present, well-defined rhombohedral crystals characteristic of calcite were produced in the presence of PEG, as shown in Figure 1a; this suggests that the presence of pure PEG has no effect on the crystal morphology. On the

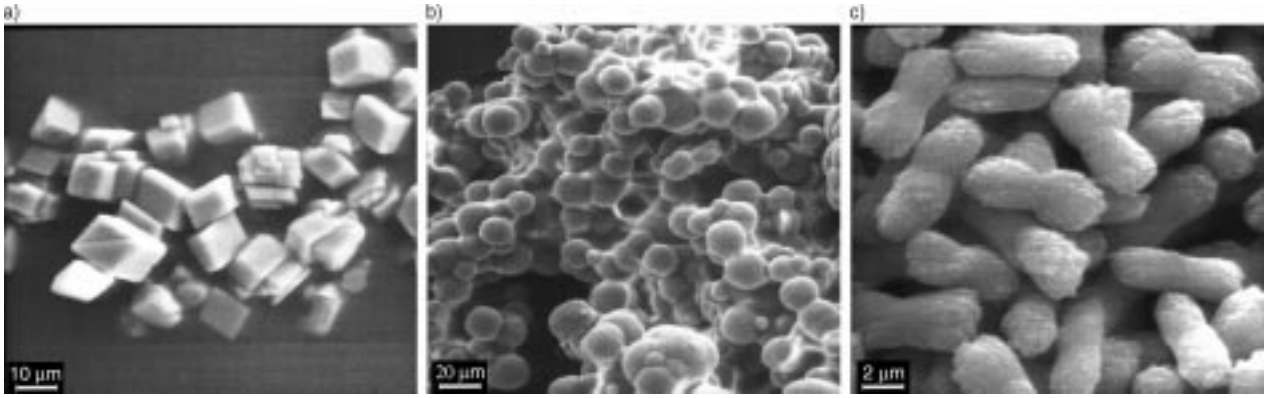


Figure 1. $CaCO_3$ particles obtained in the presence of a) PEG, b) PMAA, and c) PEG-*b*-PMAA. [polymer] = 0.2 g L$^{-1}$, [$CaCO_3$] = 8 mM, pH = 10.

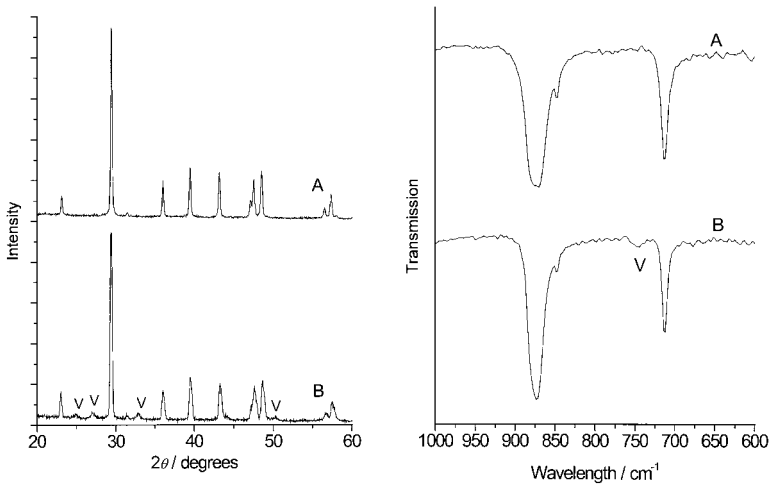


Figure 2. Left) XRD patterns and right) IR spectra of $CaCO_3$ particles obtained in the presence of PEG-*b*-PMAA. $[CaCO_3] = 8$ mM, pH = 10, [polymer] = 0.2 (A) and 0.05 g $L^{-1}$ (B). "V" denotes peaks from vaterite.

other hand, large ill-defined irregular-shaped aggregates consisting of rounded particles were obtained in the presence of PMAA (Figure 1b), typical for the strong interaction between the carboxylic acid groups of PMAA and the crystallizing $CaCO_3$, which effectively suppresses crystal growth. The corresponding XRD result suggests that the elementary globules consist of nanocrystallites of calcite with a size of about 40 nm, as revealed by line width analysis of the (104) diffraction peak. These results are basically consistent with the reported results obtained from the crystallization of $CaCO_3$ in the presence of pure PEG and PMAA with similar molecular weights.[42]

When the double-hydrophilic block copolymer PEG-*b*-PMAA was used as an additive, the crystallization of $CaCO_3$ resulted in crystals that exhibited an unusual morphology, that is, a twinned morphology with rough surfaces (Figure 1c) is found. The obtained particles are rather uniform in size and shape, with an average length and width of 6.4 and 2.1 μm, respectively. TEM pictures (not shown) reveal that both ends of the particles exhibit the faceted surfaces indicative of the stable calcite {104} faces.[19, 42] The XRD pattern shown in Figure 2 (left, curve A) exhibits only sharp calcite reflections, confirmation that the crystal superstructure is composed of well-crystallized calcite crystals. The corresponding IR spectrum (Figure 2, right, curve A) shows sharp bands at 874 and 712 $cm^{-1}$ characteristic of calcite;[12, 30] this provides further evidence for the pure calcite composition of the product.

It is interesting to note that the same type of block copolymer has been explored by Marentette et al.,[42] but under the experimental conditions they investigated, ellipsoidal calcite particles with residual calcite {104} faces at the tips were obtained, and the resulting morphology evidently depends on the reaction conditions. Such twinned, "peanut-like" particles of Mg-containing calcite can be produced relatively simply in the presence of $Mg^{2+}$ ions,[47, 48] and we assume that in our case the polymethacrylic acid units block the calcite growth in a similar fashion as the $Mg^{2+}$ ions do. Peanut-like particles of pure calcite were also obtained by the microwave-activated precipitation of $CaCO_3$ from homogeneous Ca-citrate-complexed solutions,[49] and, again, it has been assumed that the citrate blocks the growth centers in a similar fashion.

On the other hand, the found morphologies do not seem to be specific for a certain crystal/modifier pair, since evidently the same modifier applied in two earlier experiments under different addition conditions and relative concentrations resulted in particles with very differerent morphologies.[41, 42] Therefore, we varied in the following both the pH and the relative concentrations to get a more detailed view into the crystallization mechanism.

**Effect of pH**: The variation of pH drastically changed the morphology of the produced $CaCO_3$ crystals, although the XRD results suggest that all the products obtained consist of calcite crystals. Figure 3 shows the SEM pictures of the products obtained under the standard conditions but at various pHs.

It can be seen that uniform dumbbell-like particles around 5.6 μm in length and 1.6 μm in width, which exhibit well-defined faceting on the outer surfaces of the dumbbells, were produced by decreasing the pH from 10 to 9.5. When the pH was further decreased to pH 9, rodlike particles with lengths up to 15 μm and aspect ratios of up to seven were obtained; these possess rhombohedral ends and faceted side surfaces. These rodlike particles are reminiscent of the rhombohedral crystals, elongated along the *c* axis, crystallized in the presence of low molecular weight phosphate-containing additives.[27]

The increase of pH to pH 10.5 and 11 resulted in the formation of a mixture of ellipsoidal particles and irregular aggregates; the results for both pH are evidently very similar. The obtained ellipsoidal particles also exhibit residual faces at the tips, apparently resembling the ellipsoidal calcite particles obtained by Marentette et al.[42] (these authors worked at pH 10, but they employed a different mixing method), but are about 2.5 μm long and therefore smaller than the reported ellipsoidal particles (average sizes larger than 10 μm).

It is observed that the particle size is at a maximum at pH 9, that is, the nucleation rate is lowest at the lowest pH. This has to be related to the influence of pH on both the protonation degree of the carboxylic acid groups in the PMAA block of the copolymer and the $CaCO_3$ supersaturation of the solution.

As known from the neutralization curve (not shown here) of the PEG-*b*-PMAA block copolymer, in the pH range 9 – 11 the carboxylic acid groups are practically completely charged and form a polyanionic chain. The remaining minor difference in protonation is presumably not relevant for changing the rate of nucleation.

On the other hand, the solution supersaturation increases with increasing pH, which is due to the hydrocarbonate/carbonate buffer equilibrium, coupled with an increasing nucleation rate of $CaCO_3$. The nucleation rate at high pH, such as 11 and 10.5, is so high that morphology control is



0947-6539/01/0701-0108 $ 17.50+.50/0 *Chem. Eur. J.* **2001**, *7*, No. 1

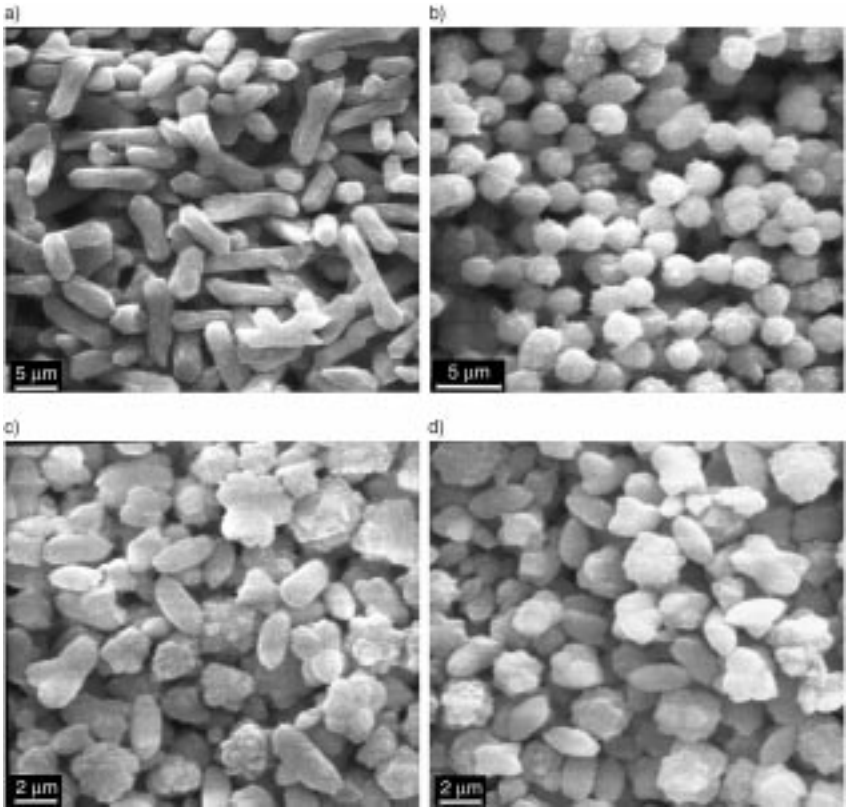


Figure 3. $CaCO_3$ particles obtained in the presence of PEG-*b*-PMAA. [polymer] = 0.2 g $L^{-1}$; [$CaCO_3$] = 8 mM; pH = a) 9, b) 9.5, c) 10.5, and d) 11.

already partially lost. Here two different types of calcite particles are formed; the TEM graphs show both ellipsoids and irregular stars.

This is in agreement with an additonal observation: precipitation takes place practically immediately at high pH, whereas with decreasing pH the induction time of $CaCO_3$ precipitation increased considerably. This is just another expression for the decrease of the supersaturation making the crystallization control by the polymer more efficient. In this context, it is should be noted that the crystals are mostly rodlike or "simple" at lowest pH, whereas the formation of twins and peanuts gets increasingly more pronounced at higher pH. This shows that not only primary nucleation, but also secondary nucleation on the side surfaces depends on the supersaturation ratio, that is, both the systematic trends of particle size and shape depend on the same set of parameters. The limit of pure rods would be obtained when primary nucleation is slowed down by the adsorption of the PEG-*b*-PMAA block copolymers at the crystal planes parallel to the *c* axis of calcite and when secondary nucleation is completely suppressed.

**Effect of the polymer concentration.** Figure 4 shows the typical EM pictures of $CaCO_3$ particles obtained at PEG-*b*-PMAA concentrations lower than the standard concentration (0.2 g $L^{-1}$). At the polymer concentration of 0.1 g $L^{-1}$, several micrometer-long rod-like or branched particles with rugged and faceted surfaces were produced (Figure 4a); this is in agreement with the XRD observations of calcite crystals.

If the polymer concentration was further decreased to 0.05 g $L^{-1}$, many small spherical particles (0.6–1.6 μm) in addition to the rugged species were obtained (Figure 4b). TEM with higher magnification reveals that the spherical particles exhibit rough surfaces and no surface faceting, while the averaged roughness is below the 50 nm scale. The XRD pattern of this sample is shown in Figure 2 (left, curve B), which shows weak and broad diffraction peaks from vaterite, a metastable polymorph of $CaCO_3$, in addition to the sharp diffraction peaks from calcite, an indication that the obtained spherical particles consist at least partly of vaterite nanocrystallites. The corresponding IR spectrum (Figure 2, right, curve B) also shows the presence of a band at 744 $cm^{-1}$, which is characteristic of vaterite,[12, 30] in addition to the bands corresponding to calcite; this provide

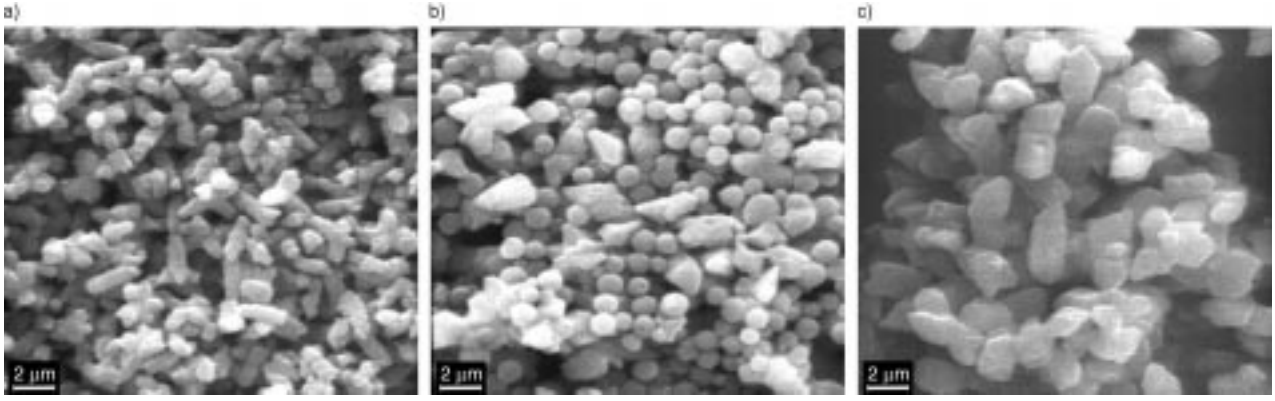


Figure 4. $CaCO_3$ particles obtained in the presence of PEG-*b*-PMAA. [$CaCO_3$] = 8 mM; pH = 10; [polymer] = a) 0.1, and b) and c) 0.05 g $L^{-1}$. Sample c) was aged for two months.

  0947-6539/01/0701-0109 $ 17.50+.50/0 

further evidence for the coexistence of calcite and vaterite in the product. In our experience, such a coexistence is usually an indication for a metastable state. Consequently, after the sample consisting of calcite particles and spherical vaterite particles was aged for two months, the spherical particles totally disappeared and only particles exhibiting well-defined surface faceting were left (Figure 4c), suggesting a complete transformation from vaterite to calcite. A similar observation has been reported for the mixture of spherical vaterite particles and calcite particles produced in the presence of an alkylethersulfonate surfactant by homogeneous precipitation, which changed into pure calcite on extended aging time.[50] It is well known that vaterite transforms readily and irreversibly into the stable calcite form through a solvent-mediated process.[51–53] We can conclude from these observations that at concentrations as low as 50 mg $L^{-1}$, the double hydrophilic polymers loose their ability to control the $CaCO_3$ morphology and modification. If the underlying process is an adsorption process, we can define an equilibrium constant $k = [\text{polymer}_{ads}]/[\text{polymer}]$ per unit area of $CaCO_3$ and, evidently, there must be a critical surface coverage $S_{cr}$ by the polymer to promote morphological changes of the growing crystal.

Ostwald-ripening and solvent-mediated recrystallization processes depend on the presence of a favourable difference in interface energy as a driving force. It must be underlined that all other structures presented before were stable against aging, that is, there is no positive interface energy difference which drives the process. This means that at coverages above $S_{cr}$, the system does not loose (or even gains) energy by exposing crystal surfaces that can adsorb polymer. It is a question of thermodynamics that at the $S_{cr}$ the interface energy is zero, while it is by definition negative at higher concentrations (all these considerations just hold for crystals being large compared to the polymer).

This goes well with the observation that stable vaterite particles (although vaterite is metastable in pure water) can be produced in the presence of organic additives that can stabilize the vaterite surface, such as bis(2-ethylhexyl)sodium sulfonate (AOT)[53] or double-hydrophilic block copolymers that contain a poly(ethyleneimine)-poly(acetic acid) block.[41] Recently, stable spherical vaterite particles (1–2 μm) were also produced in the presence of a carboxylate-terminated dendrimer.[30] It is assumed that in these cases the preferential adsorption of the polymer on vaterite relative to calcite can at least balance the relative loss in the crystallization energy.

From the fact that in our low-concentration experiment vaterite spheres were obtained, whereas only calcite crystals were produced in the control experiments in which all other experimental conditions are kept the same (without the polymer), we can speculate that well below the concentration at which PEG-*b*-PMAA is able to stabilize and modify crystals, it can play a role in initiating the nucleation of vaterite. Alternatively, the vaterite growth could be explained by a kinetic inhibition of the calcite nuclei by the limiting amount of polymer. In classical nucleation theory,[54] subcritical nuclei of all potential polymorphs are stochastically formed and dissolved, and just those nuclei which pass a critical size (defined by crystallization enthalpy *and* interface energy) can continue to grow. If a polymer lowers the interface energy of a specific polymorph (and the interface energy is lowered already below the critical surface coverage), it is this polymorph which is specifically nucleated. This concept is consistent with the recent finding that carboxylate copolymers were able to initiate the vaterite nucleation from stable supersaturated solutions through binding of the calcium ions at the ionized carboxylic groups.[11]

At higher polymer concentrations (such as 0.1 g $L^{-1}$) which maintain higher surface coverages than $S_{cr}$, the interplay of nucleation and growth becomes more complicated, because the polymorph that is most efficiently nucleated is also the one for which growth is most effectively stopped. This is presumably why we observe an induction period starting from this concentration, at which a considerable amount of $CaCO_3$ is kept stable in solution, and only calcite is grown through a slow crystallization process.

A new type of morphology was produced when the polymer concentration was increased to concentrations higher than standard (0.2 g $L^{-1}$). Figure 5 shows that dumbbell-like particles were produced in the presence of 0.5 g $L^{-1}$ PEG-*b*-PMAA, the size of which seems to be very broadly dispersed with a few large particles over 10 μm down to many small particles less than 5 μm.

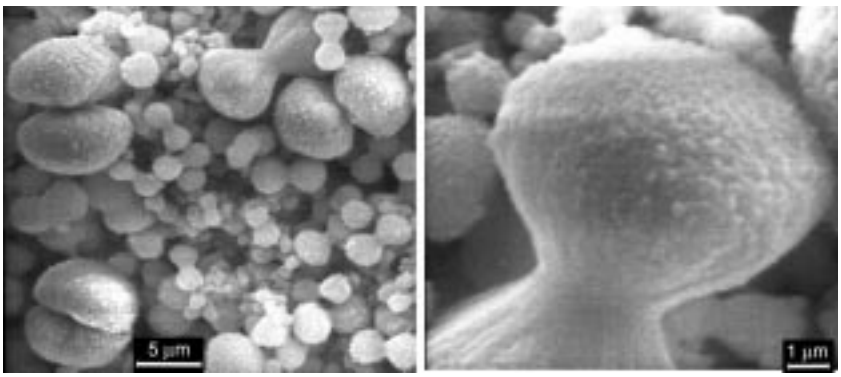


Figure 5. $CaCO_3$ particles obtained in the presence of PEG-*b*-PMAA. [polymer] = 0.5 g $L^{-1}$, [$CaCO_3$] = 8 mM, pH = 10; observed after 24 h.

The images also show the rough surfaces of the large dumbbells though the typical residual faces of calcite are hard to see. The XRD measurement, however, reveals that these particles are composed of pure calcite.

Further increase of the polymer concentration to 1 g $L^{-1}$ resulted in the extension of the heads of the dumbbells that finally close to nearly spherical particles, though smaller peanutlike particles were still present, presumably from the early stages of the dumbbell growth (Figure 6a).



0947-6539/01/0701-0110 $ 17.50+.50/0 *Chem. Eur. J.* **2001**, *7*, No. 1

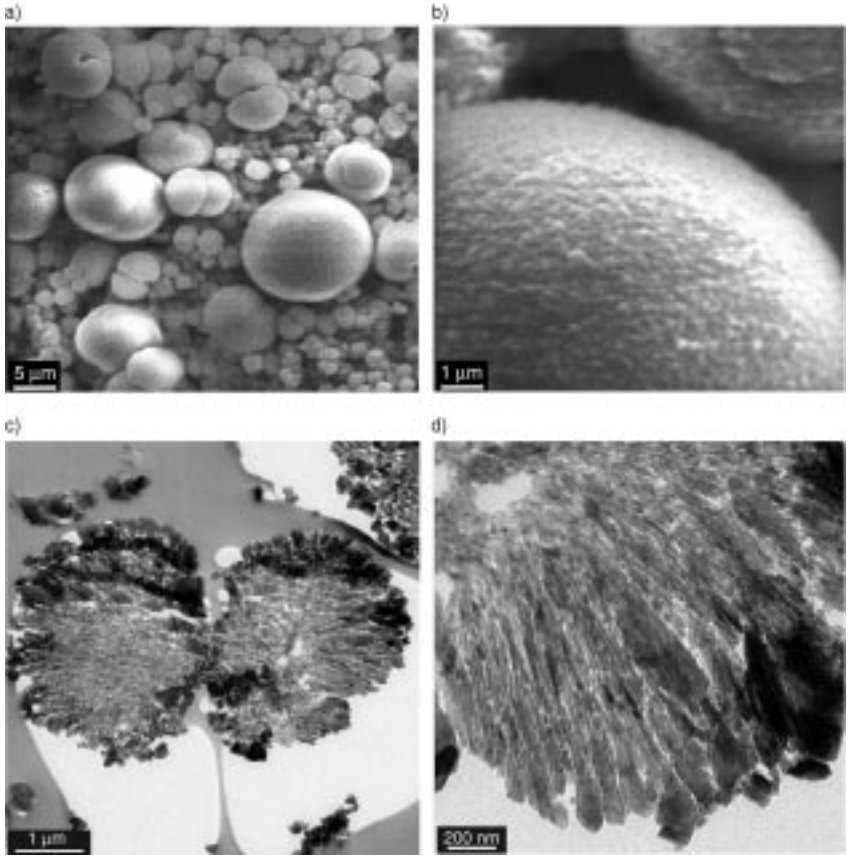


Figure 6. $CaCO_3$ particles obtained in the presence of PEG-*b*-PMAA. [polymer] = 1 g $L^{-1}$, [$CaCO_3$] = 8 mM, pH = 10; observed after 24 h. Micrographs of a dumbbell at different magnifications (a and b) and TEM pictures of a "thin-section" at different magnifications (c and d).

One can clearly observe the existence of equators or notches on the large spheres. An enlarged micrograph (Figure 6b) suggests that the large spheres also exhibit a rough outer surface. TGA analysis of the $CaCO_3$ spheres revealed only a low polymer content of 2.8 wt % in contrast to the much higher polymer contents up to 40 wt % found for spherical particles nucleated at higher polymer concentrations.[41]

The inner structure of the dumbbell-like particles was preliminarily revealed by a TEM picture from a thin-section sample. It can be seen that each dumbbell is composed of primary calcite (as revealed by WAXS) "bricks", which are rod-like at least in the outer part of the crystal. These crystallites are aligned in a way that is reminiscent of the electric-dipole field lines of a rod-shaped seed crystal discussed by Kniep for the growth of fluoroapatite[55] (see Figure 6c and d). The distance between the single-crystal building blocks is reasonably well defined (≈5 nm) and presumably houses the polymer layers. The distance between the building blocks matches well with that expected for a double layer of PEG-*b*-PMAA with the PEG block of 3000 g $mol^{-1}$.

Figure 6d also reveals that the crystallites on the outer part of the particle are bigger than those in the inner part; this is probably a secondary nucleation event that causes the observed rough surface of the dumbbells (see also Figure 5).

Other examples of spherical calcite colloids are found for the precipitation of magnesian calcite in the presence of magnesium ions[47, 56, 57] or obtained with a double-hydrophilic block copolymer as a modifier at high concentrations.[41] In all these cases, the mode of formation of the spherical superstructure remained unsolved. Again, it must be underlined that both shape and size distribution do not change even after long resident times within the mother solution, that is no Ostwald ripening or recrystallization takes place consistent with observations for $CaCO_3$ spheres obtained by another route.[57] This means that the high polydispersity results from a slow, continuous nucleation process: the same polymer that acts at very low concentrations as a nucleation agent inhibits primary nucleation at higher concentrations.

In order to gain additional evidence for the formation mechanism of the complicated calcite morphologies obtained here, we tried to follow the morphological development of the calcite spheres at different crystallization times. Figure 7 shows typical EM micrographs of the samples prepared at various early stages from the solution that yielded the calcite spheres shown in Figure 6 after 24 h.

As the solution was slightly opaque, but not obviously turbid, for the first 90 minutes SEM was not suited to characterize the structures in this inhibition period. TEM samples were prepared at 30 and 60 minutes by simply dropping a drop of the solution on carbon-coated copper grids, waiting for one minute and removing the mother solution by using filter paper. As shown in Figure 7a, only loose aggregates of evidently amorphous nanoparticles (20–30 nm, evidenced by the corresponding electron diffraction) were observed for the 30 minute-old sample.

We deduced from this observation that the actual very high supersaturation at early stages is lowered by the formation of a blockcopolymer-stabilized amorphous intermediate rather than of $CaCO_3$ nanocrystals. In other words, the crystallization inhibition operates neither through dissolved molecular species nor through molecules sequestered onto the polymer, but involves an amorphous colloidal intermediate. Similar amorphous particles were observed for the 60 minute sample although the nanoparticles constituting the aggregates seem to grow and aggregate further (Figure 7b).

After 90 minutes of aging, the solution became turbid, and large micron-sized particles were generated and characterized by SEM. From Figure 7c we can see that already at the early stages larger species (larger than 10 µm) are formed. These

big particles resemble in shape and size the big spherical calcite particles in the final blend shown in Figure 6, that is, the particles do not further grow in the remaining time of the reaction. This means that the nucleation of the calcite nanostructures from the amorphous intermediates is slow; however, the crystallization is relatively fast. The overall crystallization mechanism is in addition self-limiting: the growth stops when the outer branched or facetted shell is applied.

After 120 min, the turbidity had considerably increased; this is caused by the increase of the total number of the particles produced, as visualized by SEM. As shown in Figure 7d, more smaller dumbbells were generated, while no change in size was observed for the previously formed large spheres. Considering the presence of a large number of the smaller peanuts and dumbbells in the final product shown in Figure 6, it can be concluded that the large spheres were more favorably formed at the earlier stages of crystallization, whereas smaller dumbbells were more favorably produced at later stages, leading to the very broad distribution of the final particles. This can be attributed to the fact that either the amount of $CaCO_3$ available for crystallization (this is most probably the amorphous precursor; the molecular supersaturation is presumably constant) or the amount of polymer necessary for morphology control is lowered with time.

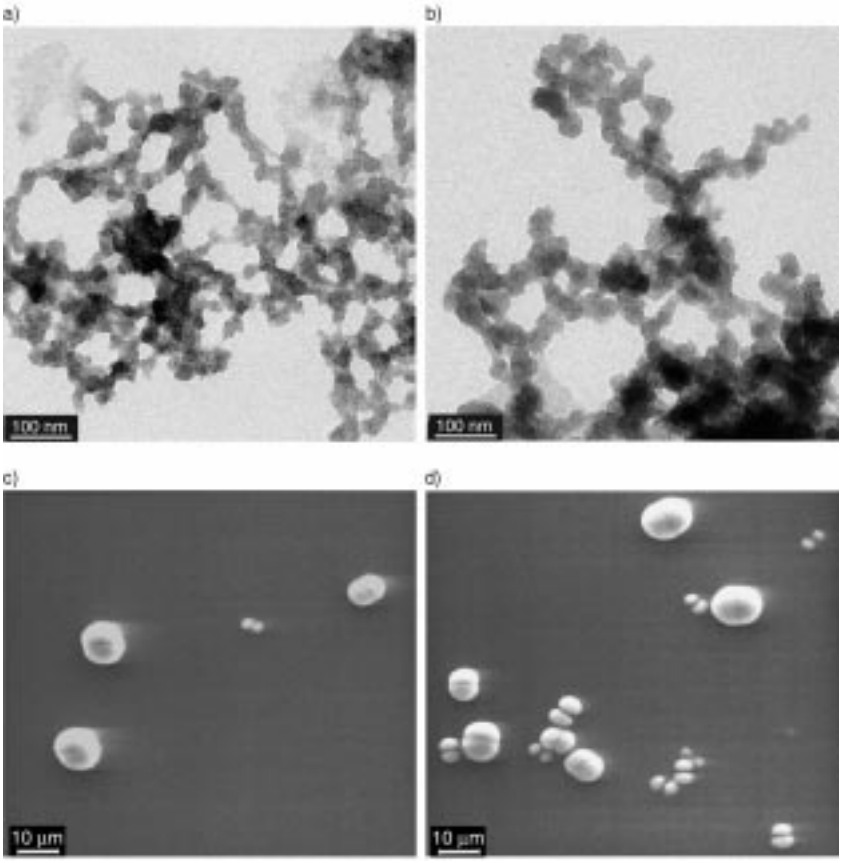


Figure 7. $CaCO_3$ particles obtained in the presence of PEG-*b*-PMAA after a) 30, b) 60, c) 90, and d) 120 min of mixing. [polymer] = 1 g L$^{-1}$, [$CaCO_3$] = 8 mM, pH = 10.

However, as TEM and SEM investigations potentially suffer from drying artifacts, we performed time-dependent dynamic light scattering on a crystallizing solution under the conditions of Figure 7 to study the growth of the crystallites in solution (see Figure 8). The mixing of the reactants was set as $t = 0$.

As it can be seen in Figure 8a, three regimes can be distinguished from the time dependence of the turbidity. Already after two minutes, the particles have a diameter of about 140 nm; this clearly states that the primary amorphous particles seen in TEM with diameters of 20 – 30 nm are already aggregated. The turbidity in region 1 (2 – 7 min) rapidly increases, which is caused by an increasing particle size and number. In region 2 (7 – 50 min), the turbidity stays constant or slightly decreases, whereas the averaged particle size still increases up to 1000 nm. This is usually the case when the increase in particle size is balanced by a decrease in the particle number, that is, the amorphous precursors either aggregate to larger units or the whole sample undergoes

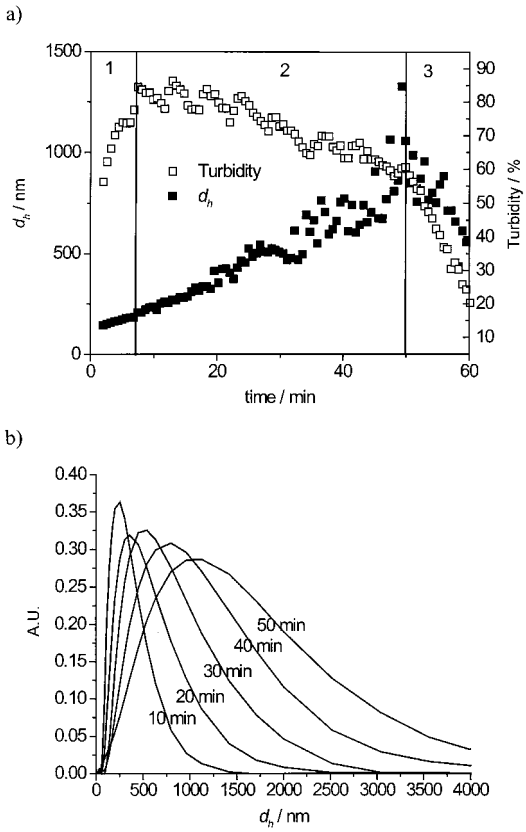


Figure 8. Time dependence of a) the hydrodynamic diameter and the turbidity as well as of b) the apparent particle size distributions.



0947-6539/01/0701-0112 $ 17.50+.50/0 *Chem. Eur. J.* **2001**, *7*, No. 1

recrystallization to a few, much larger species. It must be stated that big crystals are less visible in our scattering experiment, because we are leaving the region of Rayleigh scattering and enter the domain of Mie and Fraunhofer diffraction. Also, because of the slowing down of the relaxation processes, the sampling period is not long enough to allow for sufficient sampling statistics: the size data gets more noisy.

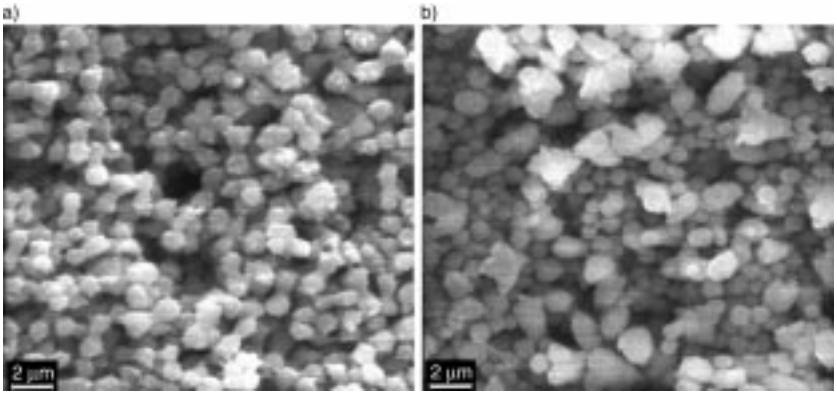


Figure 9. $CaCO_3$ particles obtained in the presence of PEG-*b*-PMAA. [polymer] = 0.2 g $L^{-1}$, pH = 10, [$CaCO_3$] = a) 4, and b) 16 mM

In region 3 ($t > 50$ min), both size and turbidity decrease; this indicates the formation of the macroscopic particles shown in Figure 7c which then precipitate and leave the scattering volume, that is, the sample is depleted of $CaCO_3$. In this period, light scattering is simply not appropriate anymore to characterize the process. It must be stated that the reproducibility of these experiments is not very high, as it must be expected for all processes with induction periods. However, all turbidity/size curves have a similar overall shape, but the starting sizes, slope, and consequently onset of crystallization vary for each experiment.

Therefore it is not suprising that the TEM observations in Figure 7 do not exactly match those in Figure 8 as the crystallization kinetics depends on mixing conditions and reactor size; however, the overall scenario seems to be supported by the solution experiments. Already after ten minutes (shortly after the steep turbidity increase in Figure 8a), the particle size distribution shows particles with sizes well exceeding the micron range. This trend is amplified with time (Figure 8b; this represents the increasing polydispersity, which is indicative of parallel continuous nucleation and growth processes that also result in the diversity of shapes (see also Figure 5 and Figure 6). However, as the smallest observed particles of about 140 nm in Figure 8a are almost completely absent after 50 min, the pool of the amorphous primary particles seems to be exhausted.

**Effect of the $CaCO_3$ concentration**: To examine the effect of the $CaCO_3$ concentration on the crystallization, the crystallization experiment was repeated at lower and higher concentrations (4 mM and 16 mM, compared with the standard of 8 mM). At the lower $CaCO_3$ concentration of 4 mM, peanutlike particles (2.2–2.8 μm) with rather rough surfaces, which are shown by the corresponding XRD result to be composed of calcite, were obtained (Figure 9a).

The obtained peanutlike particles are smaller than the particles obtained under the standard conditions and the outgrowth extent of both ends of the peanuts seems to be larger; this is attributed to the increase in the relative ratio of polymer to $CaCO_3$. Decreasing the $CaCO_3$ concentration evidently has a similar result as increasing the polymer concentration, it is just that the system has been diluted by a factor of two.

If the $CaCO_3$ concentration was increased to twice the standard concentration, that is, 16 mM, a mixture of spherical vaterite particles and less-defined calcite particles that exhibit surface faceting were obtained, an event which is very similar to the sample obtained at the standard $CaCO_3$ concentration but at a low polymer concentration of 0.05 g $L^{-1}$ (Figure 4b). Similarly, the vaterite spheres disappeared with aging, and only the calcite species remain. The observed events seem again be consistent with the decrease of the ratio of polymer and $CaCO_3$, and the overall concentration (in the restricted range covered) seems to be of secondary importance. Both $CaCO_3$ concentration experiments indicate that the relative proportion between the polymer and $CaCO_3$ concentrations is more relevant for determining the polymorph and morphology of the produced particles.

To exclude a possible effect of a higher ionic strength on crystallization (given by the free counterions of the precursors, in our case $Na^+$ and $Cl^-$), we also carried out the crystallization experiment under the standard conditions (8 mM $CaCO_3$), but with additional 16 mM NaCl. The product was essentially the same as the product obtained under the standard conditions, suggesting that the effect of ionic strength or long-range electrostatic interactions is negligible in the chosen limited range.

## Discussion

A double-hydrophilic block copolymer PEG-*b*-PMAA consisting of a binding block and a solvating block was used as an effective crystal growth modifier to control the crystallization of $CaCO_3$. Various morphologies of calcite particles, such as rod-, peanut-, and dumbbell-like, and spherical and ellipsoidal, have been successfully produced in the presence of PEG-*b*-PMAA at room temperature by a simple solution synthesis method, which provides an easy route to the biomimetic morphogenesis of calcite. The influences of important experimental factors including pH, the polymer concentration, and the $CaCO_3$ concentration on the size and morphology of the produced $CaCO_3$ particles have been investigated in detail.

The pH can influence the morphology of the calcite particles significantly with ellipsoidal and irregular particles formed at high pH, such as pH 11 and 10.5, peanut- and

dumbbell-like particles formed at medium pH, such as pH 10 and 9.5, and rod-like particles formed at low pH, such as pH 9. The effect of pH on the calcite crystallization in the presence of PEG-*b*-PMAA can be interpreted in terms of the influence of pH on both the protonation degree of the carboxylic acid groups in the PMAA block of the copolymer and the supersaturation of the solution, although the COOH groups can be considered to be completely deprotonated so that the pH effect on the solution supersaturation is the main effect. Also, the polymer concentration plays an important role in determining both the polymorph and morphology of the $CaCO_3$ particles. Spherical vaterite particles, which completely transform into calcite particles with longer aging, were produced together with calcite particles at the lowest polymer concentration. Peanut- and dumbbell-like, and large spherical calcite particles appeared successively with increasing the polymer concentration. However, the study on the influence of the $CaCO_3$ concentration on the morphology of the $CaCO_3$ particles revealed that the relative proportion between the polymer and $CaCO_3$ concentrations plays an important role in determining the characteristics of the obtained $CaCO_3$ particles rather than the absolute concentrations.

All this information can be summarized in a diagram which we call morphology map. This is shown in Figure 10. Such diagram has the useful feature to allow the prediction of morphologies that can be expected for given experimental conditions.

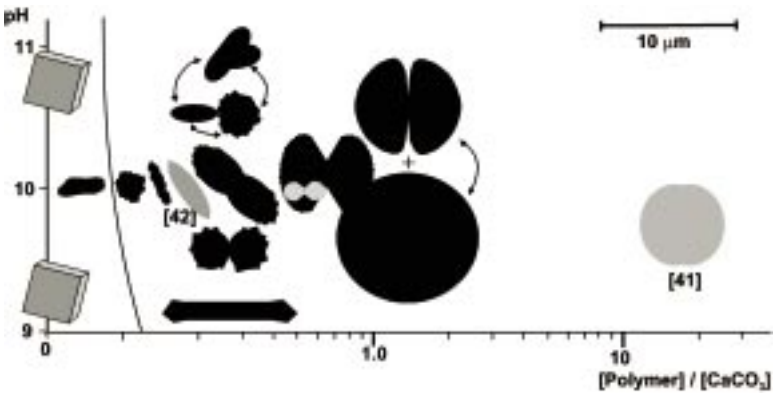


Figure 10. Morphology map of $CaCO_3$ in presence of PEG-PMAA showing the morphology dependence of $CaCO_3$ in dependence of pH and the ratio [polymer]/[$CaCO_3$] for which the unit for both concentrations is g $L^{-1}$. The particles are drawn to scale. Arrows indicate when several morphologies were observed simultaneously. Morphologies reported for the same system in refs. [41] and [42] are also included and drawn in grey.

The fact that this morphology map is general for the PEG-*b*-PMAA/$CaCO_3$ system is underlined by the fact that literature reported morphologies, which were obtained under crystallization conditions other than those applied in this study fit well into the map in Figure 10.[41, 42] The particles with calcite faces at both ends, obtained with a very similar block copolymer and reported by Marentette et al.,[42] basically represent the intermediate between the rather undefined calcite particles at very low polymer concentrations and the peanutlike particles. Also, the $CaCO_3$ spheres which we found in an earlier work in a double-jet reactor[41] are exactly the shape which we should expect for such a high [polymer]/[$CaCO_3$] ratio. This strongly indicates that the influence of the polymer on the crystallization of $CaCO_3$ at a given pH prevails over that of other parameters like reactor type, stirring speed, and so forth; this is important for the prediction of morphologies that just depend on the concentration of the polymer $CaCO_3$ and the pH.

The position of the critical surface coverage was also included in Figure 10, but it can only be considered as approximate as this value cannot be exactly measured, only its position can be concluded from the observed morphologies.

The formation of the usually equator-containing spheres that consist of pure calcite was further studied by carrying out a time-dependent crystallization experiment, which indicated that the finally observed spheres grow from amorphous nanocrystalline aggregates via dumbbell-shaped macrocrystalline intermediates with continuous nucleation of the macrocrystals.

A similar progressive growth of fluoroapatite superstructures in gelatin matrices from rods to peanuts, dumbbells, notched spheres, and finally spheres has been recently reported by Kniep et al.[55, 58] The fractal branching of successive generations, which results in the morphogenesis of the fluoroapatite spheroids, together with the overall symmetry of the self-assembled aggregates has been considered as a consequence of intrinsic electric fields, which take over control of the aggregate growth.

In our case, TEM micrographs from thin-sectioned samples of dumbbell-like particles (Figure 7c) have also indicated the alignment of rodlike nanocrystals along field lines, but not a strict fractal structure. However, a torus-shaped cavity around an elongated seed, which has been clearly observed for the fluoroapatite spheroaggregate and successfully simulated by assuming a fractal model,[58] could not be detected in our study. Nevertheless, although we only observe aggregates of amorphous $CaCO_3$ nanoparticles rather than an elongated primary seed crystal,[55, 58] the crystallization of these aggregates to dumbbell or spherical microparticles is similar to the fractal growth observed for fluoroapatite.[55, 58] However, in contrast to the fluoroapatite case, we observe secondary crystallization events on the surface of the micron-sized aggregates. Spherulitic growth can also be discussed as mechanism as the general random growth of a spherulite manifests in a linear time dependence of the particle size;[64] this indeed seems to be indicated by the results from the light scattering experiments (see Figure 8a). However, the occurrence of the dumbbell-shaped particles cannot be explained with this growth model. Nevertheless, as a precursor to spherulitic growth, the "sheaf of wheat" mechanism is discussed,[63] which in analogy to the observations of Kniep et al.[55, 58] suggests that the meeting of the opposite ends of the sheafs results in



0947-6539/01/0701-0114 $ 17.50+.50/0 *Chem. Eur. J.* **2001**, *7*, No. 1

spherical particles exhibiting equators.[59] Recently, Tracy et al. have used this mechanism to explain the formation of spherical magnesian calcite particles synthesized in the presence of both $Mg^{2+}$ and $SO_4^{2-}$ ions although it could not be proved by kinetic observations as in our case due to a very fast formation of the spheres.[57] We think our present results, which show almost all the progressive stages of evolving from aggregates of nanocrystallites via dumbbells to spheres, strongly support such a growth mechanism. The discussed growth mechanism of spheres via dumbbells that are composed of small and often rodlike primary crystallites seems to be adapted by various inorganic systems ranging from the already discussed $CaCO_3$,[41, 57] fluoroapatite[55, 58] to $BaSO_4$[44, 45] to peanutlike iron oxides obtained from amorphous precursors by a sol gel method.[60–62]

It is also interesting to note that two papers about the general crystallization phenomenon of spherulitic growth discuss growth in a locally highly viscous environment in which the crystallization is slow.[63, 64] If we consider the aggregates of amorphous nanocrystals (Figure 7), which are the precursor materials for the final spheres, the local viscosity of these aggregates can be considered to be high; this slows down the calcite crystallization and thus may be a condition for the observed spherulitic growth of the macrocrystals.

The produced calcite particles with various morphologies are promising candidates for materials due to the importance of shape and texture in determining many properties of materials.[1] The successful realization of the biomimetic morphogenesis of calcite by using a double-hydrophilic block copolymer as a crystal growth modifier extends the possibilities of previous attempts of inorganic morphogenesis[1, 2, 58] and could also have some important biological implications. The tremendous potential of block copolymers as effective tools for the controlled synthesis of inorganic crystals with unusual morphologies has been further demonstrated by the present work. It is expected that double-hydrophilic copolymers can be similarly applied to many other systems than those already successfully studied ($CaCO_3$,[41, 42] $Ca_x(PO_4)_y \cdot H_2O$,[43] $BaSO_4$[44, 45] and ZnO[46]) as an effective crystal growth modifier. Copolymers that contain more complex patterns of chemical groups may provide even more effective tools for the controlled synthesis of inorganic crystals and this possibility is currently being studied.

## Acknowledgement

We thank Anna Peytcheva for the light scattering measurements. The Max-Planck Society and the DFG (SFB 448) are acknowledged for financial support. H.C. also thanks the Dr. Hermann Schnell foundation for financial support. The Th. Goldschmidt AG, Essen is acknowledged for providing the PEG-*b*-PMAA block copolymer.

[1] S. Mann, G. A. Ozin, *Nature* **1996**, *382*, 313.
[2] H. Yang, N. Coombs, G. A. Ozin, *Nature* **1997**, *386*, 692.
[3] T. S. Ahmadi, Z. L. Wang, T. C. Green, A. Henglein, M. A. El-Sayed, *Science* **1996**, *272*, 1924.
[4] E. Matijevic, *Curr. Opin. Colloid Interface Sci.* **1996**, *1*, 176.
[5] E. Matijevic, *Chem. Mater.* **1993**, *5*, 412.
[6] S. Mann, J. Webb, R. J.P Williams, *Biomineralization, Chemical and Biochemical Perspectives*, VCH, Weinheim, **1989**.
[7] S. Mann, *Nature* **1993**, *365*, 499.
[8] S. Mann, *Biomimetic Materials Chemistry*, VCH, Weinheim, **1995**.
[9] S. Weiner, L. Addadi, *J. Mater. Chem.* **1997**, *7*, 689.
[10] M. Fritz, D. E. Morse, *Curr. Opinion Colloid Interface Sci.* **1998**, *3*, 55.
[11] E. Dalas, P. Klepetsanis, P. G. Koutsoukos, *Langmuir* **1999**, *15*, 8322.
[12] G. Falini, S. Albeck, S. Weiner, L. Addadi, *Science* **1996**, *271*, 67.
[13] D. B. DeOliveira, R. A. Laursen, *J. Am. Chem. Soc.* **1997**, *119*, 10627.
[14] S. Mann, B. R. Heywood, S. Rajam, S. J. D. Birchall, *Nature* **1988**, *334*, 692.
[15] J. M. Didymus, S. Mann, W. J. Benton, I. R. Collins, *Langmuir* **1995**, *11*, 3130.
[16] D. J. Ahn, A. Berman, D. Charych, *J. Phys. Chem.* **1996**, *100*, 12455.
[17] A. L. Litvin, S. Valiyaveettil, D. L. Kaplan, S. Mann, *Adv. Mater.* **1997**, *9*, 124.
[18] J. Lahiri, G. Xu, D. M. Dabbs, N. Yao, I. A. Aksay,J. T. Groves, *J. Am. Chem. Soc.* **1997**, *119*, 5449.
[19] D. D. Archibald, S. B. Qadri, B. P. Gaber, *Langmuir* **1996**, *12*, 538.
[20] J. Kuther, G. Nelles, R. Seshadri, M. Schaub, H. J. Butt, W. Tremel, *Chem. Eur. J.* **1998** *4*, 1834.
[21] J. Aizenberg, A. J. Black, G. M. Whitesides, *Nature* **1999**, *398*, 495.
[22] J. Aizenberg, A. J. Black, G. M. Whitesides, *J. Am. Chem. Soc.* **1999**, *121*, 4500.
[23] B. D. Chen, J. J. Cilliers, R. J. Davey, J. Garside, E. T. Woodburn, *J. Am. Chem. Soc.* **1998**, *120*, 1625.
[24] G. Falini, S. Fermani, M. Gazzano, A. Ripamonti, *Chem. Eur. J.* **1997**, *3*, 1807.
[25] G. Falini, S. Fermani, M. Gazzano, A. Ripamonti, *Chem. Eur. J.* **1998**, *4*, 1048.
[26] S. M. D'Souza, C. Alexander, S. W. Carr, A. M. Waller, M. J. Whitcombe, E. N. Vulfson, *Nature*, **1999**, *398*, 312.
[27] J. M. Didymus, P. Oliver, S. Mann, A. L. DeVries, P. V. Hauschka, P. Westbroek, *J. Chem. Soc. Faraday Trans.* **1993**, *89*, 2891.
[28] T. Kato, T. Suzuki, T. Amamiya, T. Irie, M. Komiyama, H. Yui, *Supramol. Sci.* **1998**, *5*, 411.
[29] L. A. Gower, D. A. Tirrell, *J. Cryst. Growth* **1998**, *191*, 153.
[30] K. Naka, Y. Tanaka, Y. Chujo,Y. Ito, *Chem. Commun.* **1999**, 1931.
[31] G. Xu, N. Yao, I. A. Aksay, J. T. Groves, *J. Am Chem. Soc.* **1998**, *120*, 11977.
[32] S. Zhang, K. E. Gonsalves, *Langmuir* **1998**, *14*, 6766.
[33] Y. Levi, S. Albeck, A. Brack, S. Weiner, L. Addadi, *Chem. Eur. J.* **1998**, *4*, 389.
[34] A. M. Belcher, X. H. Wu, R. J. Christensen, P. K. Hansma, G. D. Stucky, D. E. Morse, *Nature* **1996**, *381*, 36.
[35] J. Aizenberg, J. Hanson, T. F. Koetzle, S. Weiner, L. Addadi, *J. Am. Chem. Soc.* **1997**, *119*, 881.
[36] D. Walsh, S. Mann, *Nature* **1995**, *377*, 320.
[37] D. Walsh, B. Lebeau, S. Mann, *Adv. Mater.* **1999**, *11*, 324.
[38] T. Hirai, S. Hariguchi, I. Komasawa, R. J. Davey, *Langmuir* **1997**, *13*, 6650.
[39] J. Kuther, R. Seshadri, G. Nelles, W. Assenmacher, H. J. Butt, W. Mader, W. Tremel, *Chem. Mater.* **1999**, *11*, 1317.
[40] M. Sedlak, M. Antonietti, H. Cölfen, *Macromol. Chem. Phys.* **1998**, *199*, 247.
[41] H. Cölfen, M. Antonietti, *Langmuir* **1998**, *14*, 582.
[42] J. M. Marentette, J. Norwig, E. Stockelmann, W. H. Meyer, G. Wegner, *Adv. Mater.* **1997**, *9*, 647.
[43] M. Antonietti, M. Breulmann, C. Göltner, H. Cölfen, K. K. Wong, D. Walsh, S. Mann, *Chem. Eur. J.* **1998**, *4*, 2493.
[44] L. Qi, H. Cölfen, M. Antonietti, *Angew. Chem.* **2000**, *112*, 617; *Angew. Chem. Int. Ed.* **2000**, *39*, 604.
[45] L. Qi, H. Cölfen, M. Antonietti, *Chem. Mater.* **2000**, *12*, 2392.
[46] M. Öner, J. Norwig, W. H. Meyer, G. Wegner, *Chem. Mater.* **1998**, *10*, 460.
[47] S. Raz, S. Weiner, L. Addadi, *Adv. Mater.* **2000**, *12*, 38.
[48] N. Wada, K. Yamashita, T. Umegaki, *J. Colloid Interface Sci.* **1999**, *212*, 357.
[49] R. Rodriguez-Clemente, J. Gomez-Morales, *J. Cryst. Growth* **1996**, *169*, 339.
[50] L. Wang, I. Sondi, E. Matijevic, *J. Colloid Interface Sci.* **1999**, *218*, 545.

[51] N. Spanos, P. G. Koutsoukos, *J. Cryst. Growth* **1998**, *191*, 783.
[52] N. Nassrallah-Aboukais, A. Boughriet, J. Laureyns, A. Aboukais, J. C. Fischer, H. R. Langelin, M. Wartel, *Chem. Mater.* **1998**, *10*, 238.
[53] A. Lopezmacipe, J. Gomezmorales, R. Rodriguezlemente, *J. Cryst. Growth* **1996**, *166*, 1015.
[54] A. E. Nielsen, *Kinetics of precipitation*, Pergamon Press, Oxford, London, Edinburgh, New York, Paris, Frankfurt **1964**.
[55] R. Kniep, S. Busch, *Angew. Chem.* **1996**, *108*, 2787; *Angew. Chem. Int. Ed. Engl.* **1996**, *35*, 2624.
[56] S. L. Tracy, C. J. P. Francois, H. M. Jennings, *J. Cryst. Growth* **1998**, *193*, 374.
[57] S. L. Tracy, D. A. Williams, H. M. Jennings, *J. Cryst. Growth* **1998**, *193*, 382.
[58] S. Busch, H. Dolhaine, A. DuChesne, S. Heinz, O. Hochrein, F. Laeri, O. Podebrad, U. Vietze, T. Weiland, R. Kniep, *Eur. J. Inorg. Chem.* **1999**, 1643.
[59] R. B. Williamson, *J. Cryst. Growth* **1968**, *3 – 4*, 787.
[60] D. Shindo, G. S. Park, W. Waseda, T. Sugimoto, *J. Colloid Interface Sci.* **1994**, *168*, 478.
[61] T. Sugimoto, Y. Wang, *J. Colloid Interface Sci.* **1998**, *207*, 137.
[62] N. Sasaki, Y. Murakami, D. Shindo, T. Sugimoto, *J. Colloid Interface Sci.* **1999**, *213*, 121.
[63] H. D. Keith F. J. Padden, Jr., *J. Appl. Phys.* **1963**, *34*, 2409.
[64] N. J. Goldenfeld, *J. Cryst. Growth* **1987**, *84*, 601.

Received: May 19, 2000 [F2501]



0947-6539/01/0701-0116 $ 17.50+.50/0